Mineral Carbonation: Energy Costs of Pretreatment Options and Insights Gained from Flow Loop Reaction Studies

Larry Penner, William K. O'Connor, David C. Dahlin, Steve Gerdemann, Gilbert E. Rush
Albany Research Center, Office of Fossil Energy, US DOE

Abstract

Sequestration of carbon as a stable mineral carbonate has been proposed to mitigate environmental concerns that carbon dioxide may with time escape from its sequestered matrix using alternative sequestration technologies. A method has been developed to prepare stable carbonate products by reacting CO_2 with magnesium silicate minerals in aqueous bicarbonate/chloride media at high temperature and pressure. Because this approach is inherently expensive due to slow reaction rates and high capital costs, studies were conducted to improve the reaction rates through mineral pretreatment steps and to cut expenses through improved reactor technology. An overview is given for the estimated cost of the process including sensitivity to grinding and heating as pretreatment options for several mineral feedstocks. The energy costs are evaluated for each pretreatment in terms of net carbon avoided.

New studies with a high-temperature, high-pressure flow-loop reactor have yielded information on overcoming kinetic barriers experienced with processing in stirred autoclave reactors. Repeated tests with the flow-loop reactor have yielded insights on wear and failure of system components, on challenges to maintain and measure flow, and for better understanding of the reaction mechanism.

Introduction

Carbon dioxide sequestration by mineral carbonation has been investigated for the past five years at the Albany Research Center (ARC) in collaboration with the Office of Fossil Energy - Mineral Carbonation Study Group. This work has focused on the development of an *ex situ* aqueous process to convert magnesium silicate-rich ultramafic rocks and minerals, such as olivine and serpentine, to magnesium carbonates by contact with gaseous CO_2 in an aqueous solution (O'Connor et al., 2001a, 2001b, 2002). Studies within the last year have been expanded to include alternative mineral feed stocks, including calcium- and ferrous iron-rich rocks and minerals, including wollastonite and basalt. Initial studies using ultramafic rocks simplified the reaction sequence by providing high-purity mineral reactants with high concentrations of the primary cations (Ca, Fe^{2+}, Mg) necessary for precipitation of stable carbonate compounds, such as calcite ($CaCO_3$), siderite ($FeCO_3$), and magnesite ($MgCO_3$). Emphasis has been placed on the energy consumption for the overall process, which is impacted most significantly by reaction kinetics, parametrics, and efficiency. Because all three are dependent upon the mineral reactants used, some discussion of these reactants is warranted.

Mineral Chemistry

Carbonation Reactions

The alteration of Mg-bearing ultramafic rocks by natural hydrothermal fluids is known as serpentinization, and produces hydrated Mg-silicate minerals (serpentine) and, when CO_2 is available, magnesite (Eq. 1). Increasing the activity of CO_2 can by-pass the formation of the hydrated species to form the carbonates and silicic acid and/or free silica (Eq. 2). Because this reaction occurs in nature and is thermodynamically favored, it became the basis for the aqueous mineral carbonation process. Studies demonstrated that the list of primary mineral reactants could be expanded beyond the Mg-rich silicates to include the Ca- and Fe^{2+}-rich silicates as well. The theoretical carbonation reactions for the Ca-, Fe^{2+}-, and Mg-silicates are included below for reference (Eq. 1-5).

$$2Mg_2SiO_4 + CO_2 + 2H_2O \Rightarrow Mg_3Si_2O_5(OH)_4 + MgCO_3 \quad \text{Eq. 1}$$

$$Mg_2SiO_4 + 2CO_2 + 2H_2O \Rightarrow 2MgCO_3 + H_4SiO_4 \quad \text{Eq. 2}$$

$$Mg_3Si_2O_5(OH)_4 + 3CO_2 + 2H_2O \Rightarrow 3MgCO_3 + 2H_4SiO_4 \quad \text{Eq. 3}$$

$$Fe_2SiO_4 + 2CO_2 + 2H_2O \Rightarrow 2FeCO_3 + H_4SiO_4 \quad \text{Eq. 4}$$

$$CaSiO_3 + CO_2 + 2H_2O \Rightarrow CaCO_3 + H_4SiO_4 \quad \text{Eq. 5}$$

Carbonation Potential

A key theoretical yardstick for the value of a particular mineral reactant for mineral carbonation is its carbonation potential. The carbonation potential for a rock or mineral was described by Goff et al. (2000) regarding the hydrated magnesium silicate serpentine [$Mg_3Si_2O_5(OH)_4$]. Goff used the molar concentration of Mg in a serpentine sample to calculate the theoretical number of moles of CO_2 that could be converted to magnesite ($MgCO_3$) by reaction with the serpentine. This method was modified for the current study to include the cations Ca and Fe^{2+} in the calculation, because all three cations can potentially form stable carbonate compounds. The modified method thus permits the calculation of the carbonation potential for the alternative mineral feed stocks studied (Table 1). The carbonation potential, R_{CO2}, was calculated from the total molar concentration of Ca, Fe^{2+}, and Mg in the feed, and is defined here as the mass ratio of rock or mineral necessary to convert a unit mass of CO_2 to the solid carbonate (Eq. 6). By this definition, a low R_{CO2} is preferable to a high R_{CO2}.

$$R_{CO2} = \frac{100}{\left(\sum Ca^{2+} + Fe^{2+} + Mg^{2+}\right) MW_{CO2}} \qquad \text{Eq. 6}$$

Where:
$\sum Ca^{2+}+Fe^{2+}+Mg^{2+}$ = The sum of the molar concentrations for the specified cations.
MW_{CO2} = Molecular weight of CO_2.

Carbonation Reactivity

While the R_{CO2} is an inherent property of a rock or mineral, based strictly on its chemical composition, the carbonation reactivity of that rock or mineral is dependent on numerous factors, including the mineral composition, pretreatment, and solubility at the specific carbonation conditions of time, temperature, and pressure.

An evaluation of the relative sequestration reactivity for the specific mineral feed stocks studied is also included in Table 1. The reactivity of the various feed materials was measured as the extent of reaction, R_X, or the percent stoichiometric conversion of the Ca-, Fe^{2+}-, and Mg-silicates to their carbonate counterparts (Eq. 7).

Table 1. Mineral chemistry, carbonation potential, and reactivity.[1]

Rock/mineral group	Mineral	Formula	Concentration, wt pct				R_{CO2}[2]	ε_A[3], %	R_x[4], %
			Feed			Prod.			
			Ca	Fe^{2+}	Mg	CO_2			
Feldspar	Anorthite (An)	$CaAl_2Si_2O_8$	10.3	3.1	4.8	1.9	4.4	23	9
Serpentine	Antigorite (Ant)	$Mg_3Si_2O_5(OH)_4$	<0.1	2.4	24.6	24.2	2.1	47	92
Pyroxene	Augite (Aug)	$CaMgSi_2O_6$ + (Fe,Al)	15.6	9.6	6.9	11.1	2.7	37	33
Basalt	An, Aug, Mt, Ol		6.7	6.7	4.3	2.9	4.9	37	15
Olivine (Ol)	Fayalite (Fa)	Fe_2SiO_4	0.6	44.3	0.3	19.2	2.8	36	66
Olivine (Ol)	Forsterite (Fo)	Mg_2SiO_4	0.1	6.1	27.9	29.7	1.8	56	81
Serpentine	Lizardite (Liz)	$Mg_3Si_2O_5(OH)_4$	0.3	1.5	20.7	16.0	2.5	39	40
Oxide	Magnetite (Mt)	Fe_3O_4	0.6	21.9	0.3	1.5	5.5	18	08
Ultramafic	Talc	$Mg_3Si_4O_{10}(OH)_2$	2.2	9.2	15.7	5.2	2.8	36	15
Ultramafic	Wollastonite (Wo)	$CaSiO_3$	31.6	0.5	0.3	22.9	2.8	36	82

[1] Carbonation test conditions: 80% -37 μm feed; 1 hour; 185˚C; P_{CO2}=150 atm; 15% solids; 0.64 *M* $NaHCO_3$, 1 *M* NaCl.
[2] Mass ratio of ore necessary to carbonate unit mass of CO_2.
[3] % weight gain assuming 100% stoichiometric conversion of the available cations to the carbonates.
[4] Reaction efficiency, % stoichiometric conversion of Ca, Fe^{2+}, and Mg cations in silicate feed to carbonate.

$$R_X = \frac{X_{CO2}}{\varepsilon_A\left(1 - X_{CO2}\right)} \qquad \text{Eq. 7}$$

Where:
X_{CO2} = CO_2 concentration in the solid products in weight percent.
ε_A = Percent weight gain assuming 100% stoichiometric conversion of the available cations to the carbonates.

Due to the variability in mineral solubility, partial pressure of CO_2 (P_{CO2}) sensitivity, and precipitation kinetics, it was not practical to conduct all tests at a standardized set of pretreatment and carbonation conditions. Thus, the R_X values reported in Table 1 generally represent the best results achieved for each mineral reactant to date. The standardized test conditions are included as a footnote to the table. Variations from the standard conditions are noted below. For example, the wollastonite and forsterite exhibit comparable R_X, but both required an ultra-fine grinding pretreatment stage to achieve those reaction efficiencies. In addition, the P_{CO2} for the wollastonite carbonation is much lower than that for the forsterite, at 40 atm versus 150 atm, respectively. Countering the reduced P_{CO2} for wollastonite, however, is its higher R_{CO2} relative to forsterite. Because Ca is a much heavier element than Mg, the Ca-bearing silicates have a lower molar concentration of cations suitable for carbonation per unit mass, and thus a higher R_{CO2}. Both these factors have a significant impact on the process economics, which are discussed in greater detail in a later section.

Antigorite serpentine has the second lowest R_{CO2} and the highest R_X of the minerals investigated. However, a heat pretreatment stage was necessary to achieve this degree of reactivity. Lizardite serpentine underwent an identical heat treatment stage to achieve the reported R_X, although to less effect. The lower reactivity of the non-heat treated hydrated magnesium silicates is evident in the R_X of 15% reported for talc. Heat treatment proved an effective activation methodology for the hydrated minerals. However, as with the ultra-fine grinding used to activate olivine and wollastonite, heat treatment has a significant impact on the process economics and CO_2 balance.

Finally, the mafic rocks and/or minerals, including basalt, which is comprised in part of varying concentrations of anorthite, augite, magnetite, and olivine, all tend to exhibit the lowest R_X and the highest R_{CO2}. The anorthite and augite tests included the ultra-fine grinding stage, but were conducted for longer carbonation times (6 hours) than the standard 1 hour carbonation time, thus the R_X for 1 hour for both would be lower than shown. Although the fayalite and magnetite tests were also conducted for 6 hours rather than the standard time, their R_X are believed to be comparable to the others because neither underwent the ultra-fine grinding stage.

Mineral Pretreatment

Activation of the mineral reactants has been achieved by both thermal and mechanical means, although the mechanism for this activation is not clearly understood. Because most mineral dissolution reactions are surface controlled, it is possible that the two pretreatment methods proved successful primarily due to increased surface area. Mechanical pretreatment reduces the mean particle size of the minerals, while thermal pretreatment removes chemically-bound water, which may increase the porosity and the resulting surface area. Zhang et al. (1996) provided some discussion of the enhancement of Mg silicate solubility by mechanical means, while McKelvy et al. (2002) and Chizmeshya et al. (2002) described thermal activation and computational modeling studies, respectively, conducted at Arizona State University, a collaborating laboratory with ARC. All suggest that the activation is due to destruction or disordering of the mineral lattice. It is likely that both phenomena are responsible to some degree for the improvements in mineral reactivity achieved by pretreatment. However, because the energy penalty necessary to achieve such activation is most critical to the viability of any mineral-carbonation process, the following discussion focuses on the energy consumption for the various mineral pretreatment options, rather than the root causes for enhanced reactivity.

Mechanical Activation

Mechanical activation was investigated by use of conventional rod and ball milling techniques, as well as ultra-fine grinding using a scalable stirred-media detritor (SMD) mill. The Work Index (grinding energy) necessary for specific size reduction was calculated for olivine and the two serpentine minerals, using data derived from pilot-scale comminution tests conducted on the ores and the formula described by Bond (1952). Energy consumption for ultra-fine grinding was determined by direct measurement from

the SMD mill. Four test series were conducted on the primary mineral reactants to evaluate the sensitivity of mineral reactivity (R_X) to grinding energy (Figure 1).

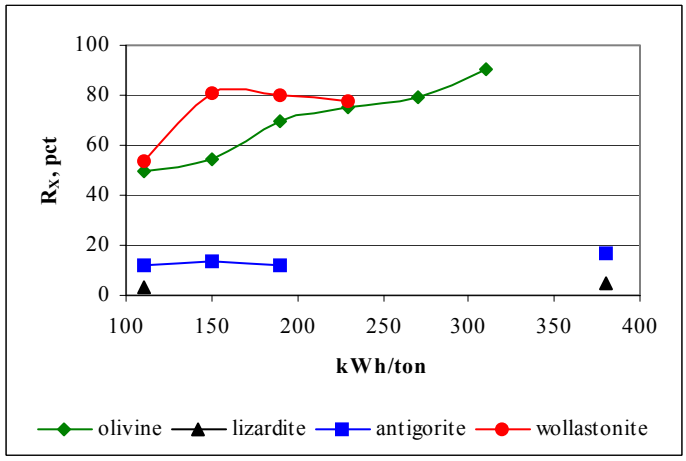

Figure 1. Grinding energy versus Rx.

The carbonation test conditions varied by mineral, using the best demonstrated reaction parametrics: 1 hour duration (all minerals); 185°C (olivine), 155°C (serpentines), 200°C (wollastonite); P_{CO2} of 150 atm (olivine and serpentines), 40 atm (wollastonite); carrier solution of 1 *M* NaCl, 0.64 *M* $NaHCO_3$ (olivine and serpentines), distilled water (wollastonite). While olivine showed a nearly linear relationship between mechanical energy input and R_X, wollastonite activation peaked at a much lower energy input, with no gain at higher energies. In contrast, both serpentine minerals show virtually no increase in R_X at energies up to nearly 400 kW•h/ton. Additional studies using a laboratory-scale attrition-grinding mill showed significant activation of the serpentines, but the estimated energy consumption was extremely high, and activation of serpentine by mechanical means alone appears impractical.

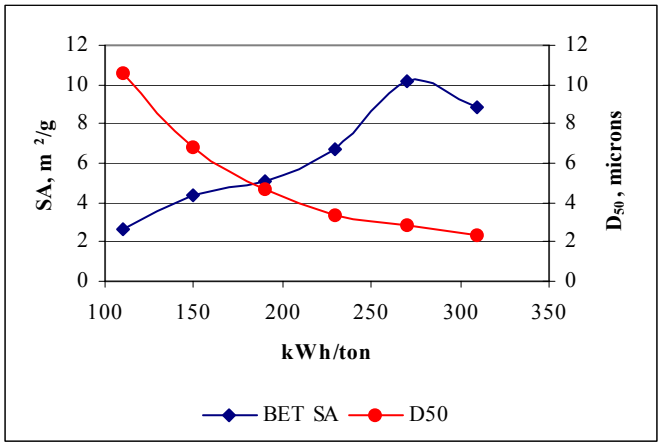

Figure 2. Olivine grinding energy versus particle size and surface area.

The relationship between particle size and surface area versus mechanical energy input was also examined for the olivine ground products (Figure 2). Particle size is represented by the D_{50} (50% finer than specified diameter) as determined by an X-ray absorption sedimentation method. Not surprising is the fact that olivine particle size decreases while reactivity increases with increasing grinding energy. Surface area measurements by BET N_2 adsorption increase from 2.6 to 10.2 m^2/g over this same series. Because all carbonation tests were conducted for 1 hour, reaction rates cannot be derived from these data, but it is likely that the increased surface area accelerated the dissolution rate of the mineral, leading to further extent of reaction within the 1-hour test time.

Thermal Activation

Thermal activation of the hydrated Mg-silicate species was accomplished by the addition of a heat treatment stage in the mineral pretreatment process. An effective heat treatment methodology was developed experimentally and confirmed by differential thermal analysis and thermal gravimetric analysis (DTA/TGA) of the antigorite serpentine ore sample (Figure 3).

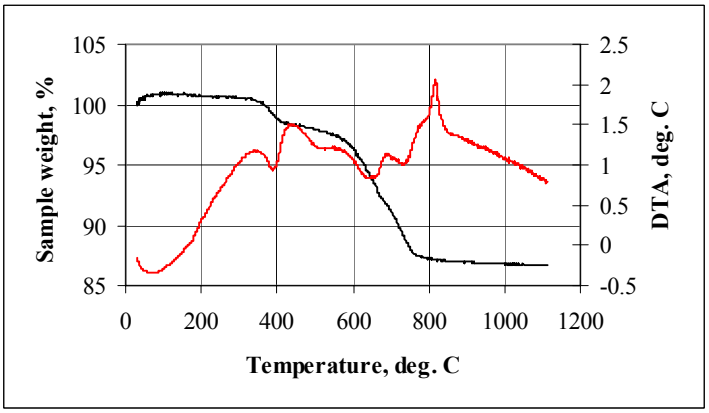

Figure 3. DTA (red) & TGA (black) for antigorite.

The most effective heat-treatment temperature determined experimentally was approximately 630°C. This is reflected in the TGA plot, which shows the most significant weight loss, due to

dehydroxylation or removal of the chemically-bound water, initiating at about 600°C. The DTA plot shows an endotherm in this temperature range centered on approximately 650°C, which corroborates the experimental data derived from bulk heat treatment of the ore. A second endotherm evident on the DTA plot occurs at about 390°C, coinciding with a weight loss of roughly 2% based on the TGA. This may be indicative of brucite [$Mg(OH)_2$] dehydroxylation, which occurs at roughly 375°C. X-ray diffraction (XRD) analysis of the same sample identified brucite as a minor phase (1-10%). DTA/TGA of the lizardite samples showed no similar weight loss or endotherm around 400°C, suggesting that brucite is absent from those ores. Because Mg-hydroxide species are far more reactive than Mg silicate, the presence of brucite in the antigorite sample may help explain the higher R_x achieved for that serpentine compared to the lizardite variety.

A great deal of study has focused on serpentine activation, both recently within the DOE Mineral Carbonation Study Group, and prior to the current research. Barnes et al. (1950) described extensive studies on the utilization and heat activation of Texas serpentine. Zhang et al. (1997) reported on the enhancement of acid extraction of Mg and Si from serpentine by mechanochemical treatment, although the 6-hour grinding times utilized likely make the methodology extremely energy-intensive. From a process standpoint, the energy consumption required for activation is more significant than the methodologies themselves, which led to an effort to determine the relative energies for thermal activation of the serpentine minerals used in the current study.

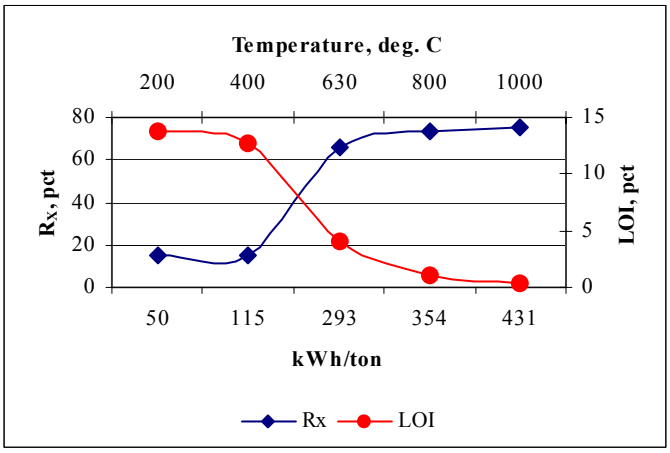

Figure 4. Antigorite heat treatment energy versus Rx.

The theoretical energy required for the heat activation process must include the energy to heat the mineral to the specified temperature and the enthalpy of dehydroxylation. The latter includes the energy to decompose the serpentine, removing the hydroxyl molecule and producing a pseudo-amorphous silicate phase. Thermodynamic data reported by King et al. (1967) was used to calculate the effective heat capacities at temperature for antigorite serpentine. The theoretical energy required to heating the mineral to the specified temperature was calculated by Equation 8.

$$Q = C_P \Delta T \qquad \text{Eq. 8}$$

Where:
Q = heat, cal/mol
C_P = cal/K•mol @ temperature T_1, (K)
ΔT = $T_1 - T_0$ (298K)

Quantitative DTA analysis was utilized to determine the dehydroxylation energies (E_d) for antigorite and lizardite serpentine, which were reported by Govier and Arnold (2004) to be approximately 95 and 131 kJ/mol, respectively. Combining the C_P data derived for antigorite serpentine coupled with these mineral-specific E_d values results in the total theoretical energy requirement for the heat-activation process. For example, heat treatment of the serpentine at 630°C (C_P = 89.26 cal/K mol) requires 206 kW•h/ton to heat the mineral, while dehydroxylation of the antigorite and lizardite requires an additional 87 and 120 kW•h/ton, respectively. Total energy consumption for the heat treatment process is thus 293 and 326 kW•h/ton, for antigorite and lizardite, respectively.

A series of heat treatment tests was conducted over a range of 200-1,000°C at 200°C intervals to evaluate the effect of heat-treatment temperature on antigorite serpentine reactivity. The reported energy values for the heat-treatment process represent the thermal energies required at each temperature as calculated by the method described above (Figure 4). The energies at the 200°C and 400°C heat

treatment temperatures do not include the E_d because dehydroxylation does not occur at temperatures below approximately 600°C.

The Loss-on-Ignition (LOI) curve was added to Figure 4 to emphasize the relationship between carbonation reactivity and effective removal of bound water. The LOI continues to decrease at temperatures above 630°C, although R_X increases only slightly, thus the added energy is not considered cost-effective. Barnes et al. (1950) identified an effective zone for activation that ranges from roughly 600-725°C, distinguished by an amorphous XRD pattern of the activated serpentine. McKelvy et al. (2001) described a meta-stable serpentine phase that forms in roughly the same temperature range, and suggested that heating above 800°C is undesirable, because this leads to a phase transformation to the non-hydrated Mg-silicate phases, forsterite and enstatite. This phase transformation is marked by an exotherm at just over 800°C (Figure 3).

Energy Consumption

Using the energy data compiled during the mechanical and thermal activation studies, a compilation of comparative energy consumption values was prepared for each of 7 ultramafic mineral carbonation regions (Table 2). For a discussion on location and content of these domestic mineral sources see O'Connor et al. (2004). The feed material histories are summarized in the first three columns of the table, with a code specific to each material included in column 4. This code is used in subsequent tables to conserve space. The rest of the table includes the energy consumption values determined for the various mineral pretreatment methodologies by stage.

For example, crushing energy for all materials is estimated at 2 kW•h/ton, based on mining cost data produced by the U.S. Bureau of Mines (1987). Ore grade is assumed to be 100% for the Twin Sisters olivine and all serpentine mineral districts (Regions 1-4, 6), based on first-hand observation of several of the mining operations, which are essentially open-pit quarries that require no concentration steps. However, laboratory analysis of olivine samples collected from the Asheville Mining District (Region 5) identified alteration minerals, serpentine and talc, with an estimated ore grade of 70% olivine. Bench-scale tests conducted on the Region 5 olivine ore indicated that gravity separation could be an effective beneficiation process, with an energy penalty of approximately 2 kW•h/ton. It is assumed that the beneficiation step would be conducted following the first grinding stage, which appears to provide sufficient liberation of the olivine from the alteration products based on the laboratory studies. Thus, the grinding energy for the stage 1 grind is based on the tonnage of raw ore processed, while subsequent pretreatment energies are based on processing the olivine concentrate.

Table 2. Energy consumption by feed material and specific pretreatment methodology.

Feed Material History				Pretreatment Energy Consumption, kW•h/ton						
						Grinding			Heat	
Region	Ore mineral & grade	Pretreatment methodology	Code	Crush.	Bene.	Stage 1	Stage 2	Stage 3	treatment	Total
1	Olivine, 100%	Ball mill (-200 mesh)	1A	2		11				13
		Ball mill (-400 mesh)	1B	2		11	70			83
		SMD mill	1C	2		11	70	150		233
2-4	Serpentine, 100% (lizardite)	Ball mill (-200 mesh)	2-4A	2		11				13
		Heat treatment (-200)	2-4B	2		11			326	339
5	Olivine, 70%	Ball mill (-200 mesh)	5A	2	2	15				19
		Ball mill (-400 mesh)	5B	2	2	15	70			89
		SMD mill	5C	2	2	15	70	150		239
6	Serpentine, 100% (antigorite)	Ball mill (-200 mesh)	6A	2		11				13
		Heat treatment (-200)	6B	2		11			293	306
		Heat treatment (-400)	6C	2		11	70		293	376
7	Wollastonite, 50%	Ball mill (-400 mesh)	7A	2	4	21	70			97
		SMD mill	7B	2	4	21	70	70		167

Virta (2001) reported wollastonite grade in the Region 7 deposits at 40-60%. Information provided with samples from the largest wollastonite mining operation in Region 7 described a two-stage concentration process, including size separation to remove calcite and magnetic separation to remove garnet. The wollastonite ore grade was assumed to be 50% for the subject calculations, and a beneficiation energy penalty of 4 kW•h/ton was added to the overall pretreatment energy consumption figure. As with the Region 5 olivine beneficiation, the size and gravity separation steps would be conducted on the raw wollastonite ore following the first-stage grind, which increases the grinding energy for that stage accordingly, compared to the non-beneficiated ore materials. Subsequent pretreatment energies are based on processing the wollastonite concentrate.

This compilation was used to calculate the theoretical parasitic energy loss from the power plant, based on the measured mechanical/thermal activation energies and experimental carbonation data. The basis for this calculation was a 1 GW coal-fired power plant, burning coal with an as-fired heat value of 12,500 Btu/lb and carbon content of 74%, at 35% plant efficiency. The CO_2 emissions of 25.4 kt/day were then used to calculate the daily ore requirement to sequester 100% of the CO_2 emissions at the R_{CO2} and demonstrated R_X of each mineral reactant in a single pass through the carbonation reactor. The results are included in Table 3.

Table 3. Parasitic energy loss by pretreatment.

Feed Code	R_{CO2}	R_X, %	Ore/conc., kt/day	Pct total plant energy
1A	1.8	16	286	15
1B	1.8	61	75	26
1C	1.8	81	56	55
2-4A	2.5	9	706	37
2-4B	2.5	40	158	222
5A	1.8	16	286	22
5B	1.8	61	75	28
5C	1.8	81	56	56
6A	2.1	12	445	24
6B	2.1	62	86	110
6C	2.1	92	58	90
7A	2.8	43	165	67
7B	2.8	82	87	61

While the daily ore requirements decrease dramatically with increased mineral activation, the coincident parasitic energy loss on the power plant becomes problematic. The latter is critical because it provides an estimate of the CO_2 balance, based on the pretreatment energies only. For example, the 15% of total plant energy necessary for pretreatment methodology 1A (minus 200-mesh Twin Sisters olivine) indicates that the CO_2 avoided is approximately 85% for that feed material at that degree of pretreatment. This assumes that the energy required for the pretreatment operation is generated by burning the same coal at the same efficiency as stated for the power plant. Adding the sequestration plant energy requirement decreases the CO_2 avoided even further. Parasitic energy losses exceeding 100% indicate that the CO_2 avoided is negative, meaning that more CO_2 is emitted by the pretreatment operation than is sequestered. These problems are most acute for the thermal-activation operations on the serpentine minerals, but the high energy consumption for the mechanical activation operations on the olivine and wollastonite minerals are also problematic.

The improved reactivity achieved by the additional pretreatment operations is negated for the most part by the higher energy demand. However, the higher ore requirements at the lower pretreatment energies require massive increases in mining output, exceeding the available resources in some regions. These calculations assume a single pass of the mineral through the carbonation plant; the successful addition of a recycle stream could reduce the virgin ore demand significantly.

Table 4. Physical properties of the pretreatment products.

Feed Code	D_{80}, μm	D_{50}, μm	BET SA, m^2/g
1A	75	20	5
1B	37	14	NA
1C	10	3	7
2-4A	75	19	32
2-4B	NA	22	11
5A	NA	NA	NA
5B	NA	NA	NA
5C	NA	NA	NA
6A	75	13	9
6B	NA	NA	NA
6C	37	17	19
7A	NA	NA	NA
7B	NA	NA	NA

Physical Properties

Several physical properties of the specific pretreatment products were measured for comparison. The results included in Table 4 provide some insight into the mechanisms impacting the activation phenomena.

The D_{80} values correspond with the size reduction targets for the stage-1 grinding operations. The minus 200-mesh ball mill product from pretreatment methodology 1A represents material that is 80% finer than 75 μm, and so on. The further reduction in particle diameter with each succeeding stage of grinding is reflected in both the D_{80} and D_{50} values. Particle diameters below 10 μm may significantly reduce if not eliminate diffusion limitations at the mineral specific carbonation reaction conditions, while coincident increases in surface area improve the mineral dissolution kinetics. Both phenomena improve R_X, although at significant energy penalty, as specified in Table 3.

The heat-activation process on the serpentine minerals tended to increase the mean particle diameter for both minerals, but with opposite impacts on the surface areas. Lizardite (2-4B) surface area decreased by nearly 300% after heat treatment, while antigorite (6B and C) surface area increased by over 200%. These variations in surface area may help to explain the much higher reactivity of the heat-activated antigorite compared to that of the heat-activated lizardite. The reason for the variable surface areas after removal of the bound water is likely tied to the different lattice structures of the two minerals, a discussion beyond the scope of this paper.

Carbonation Costs

The final carbonation cost determined in the NETL feasibility study by Lyons et al (2003) was $69 per ton CO_2 sequestered for the baseline olivine process described above. This baseline process applies directly to ultramafic (olivine) mineral carbonation in Region 1. However, the R_X values reported in the subject study were achieved in 1-hour reactor residence times rather than the 2-hour residence time assumed for the NETL study. Thus, the sequestration cost was lowered to $54 per ton CO_2, based on the reactor residence-time sensitivity analysis. Dividing the modified sequestration cost of $54 per ton CO_2 by the ore demand value (R_{CO2}/R_X) for the ore in Region 1 results in a cost of ~$18 per ton ore. It was necessary to derive the sequestration cost per ton of ore in order to account for variations in the pretreatment operations, which are mineral-specific and are reported as an energy cost per ton of ore in Table 2. This made it possible to determine an adjusted carbonation cost, including the pretreatment and sequestration costs, for each of the ultramafic mineral-carbonation regions. Multiplying the final adjusted cost per ton of ore by the calculated total ore demand provides the total carbonation cost for each region. Dividing the total calculated regional CO_2 emissions by the total carbonation costs provides the carbonation cost per ton of CO_2 sequestered. Using this method, the estimated carbonation costs were determined for each ultramafic mineral carbonation region and are reported in Table 5.

The adjustments made to account for variations in ore grade, grinding intensity, and carbonation conditions were mineral- and/or region-specific. Details of the adjustments were reported by O'Connor et al (2004). Table 5 includes two sets of carbonation costs. The first set is for what has been termed standard pretreatment, with the associated costs described above. The second set of carbonation costs

Table 5. Annual coal consumption, energy generation, CO_2 emissions, ore requirements, and carbonation costs by ultramafic mineral carbonation Region.

Region	Coal, Mt	Heat value, Btu/lb[1]	Energy, GW•h (x 1000)	CO_2 seq., Mt[2]	Ore demand, Mt		Sequestration costs							
							$/ton ore[3]		$, billions		$/ton CO_2 seq.		$/kW•h	
					std.	act.	std.	act.	std.	act.	std.	act.	std.	act.
1	7	12300	18	18	53	40	18	26	1.0	1.1	54	59	0.06	0.06
2	4	11030	9	10	302	64	15	44	4.4	2.0	427	199	0.49	0.23
3	4	11030	9	10	303	71	15	44	4.4	2.3	427	222	0.49	0.25
4	31	11360	72	72	2117	446	15	44	30.7	14.3	427	199	0.43	0.20
5	69	13080	184	187	552	416	19	27	10.3	11.1	55	59	0.06	0.06
6	85	13080	320	231	3971	527	15	48	57.7	17.9	250	78	0.26	0.08
7	28	13080	75	76	492	259	14	19	6.9	4.8	91	64	0.09	0.06
Total	228		687	604	7790	1823	15	37	115.4	53.7	191	89	0.20	0.09

[1] As-fired coal heat value based on primary coal used in each Region, after Babcock & Wilcox (1998).
[2] Total CO_2 emissions based on coal consumption and carbon content by region as described by O'Connor et al (2004); CO_2 sequestered assumes sequestration of 100% of emissions.
[3] Carbonation cost per ton of ore, derived from NETL feasibility with adjustments described in text.

refers to the activated pretreatment methodologies, which were defined previously. Ultrafine grinding was utilized for activation of the olivine and wollastonite ores and/or concentrates, while heat treatment

was utilized for activation of the serpentine ores. The grinding energy necessary to grind beyond the 400-mesh (37 μm) size assumed in the NETL study, or the energy required to add a heat-treatment step for the serpentine ores, was reported in Table 2. Using these energies and the $0.054 per kW•h basis from the NETL study, the adjusted carbonation costs per ton ore and per ton CO_2 were calculated. As described above, the adjustments to the pretreatment costs ignore capital costs for the processing equipment, thus the costs here are lower than would be expected. While it is recognized that these costs could be significant, perhaps as high as the operating costs, proper scaling of equipment would require separate feasibility studies for each region that are not considered practical at this time. They may not be necessary, because the estimated values included in Table 5 are intended to provide a relative comparison of carbonation costs between mineral reactants rather than absolute carbonation costs.

CO_2 Balance

The total energy balance was used for calculation of the carbonation cost per kW·h, and it was also necessary to determine the net CO_2 avoided by the mineral-carbonation process. The NETL study determined a total energy demand for the baseline process. This baseline value was adjusted to account for the lower energy consumption required for the 1-hour carbonation (instead of 2 hours) residence time and the coarser particle size (<200 mesh instead of <400 mesh) used for the non-activated ores.

Assuming the energy required for the mineral-carbonation process was supplied by the same coal-fired power plants generating the CO_2 to be sequestered, the CO_2 generated by the mineral-carbonation process can be calculated. Subtracting the latter from the total CO_2 sequestered results in the net CO_2 avoided. The CO_2 avoided with the standard pretreatment methodology for all seven regions, is roughly 76% of the total CO_2 sequestered. Carbonation costs increase accordingly, to roughly $80 and $112 per ton of CO_2 avoided for the two olivine ores and the wollastonite ore, respectively. Carbonation costs for the non-heat-activated antigorite and lizardite serpentine ores increase to roughly $300 and $500 per ton CO_2 avoided. With the addition of the mechanical activation step for the olivine and wollastonite ores, the CO_2 avoided is reduced to roughly 40% of the CO_2 sequestered. The addition of the heat activation step for the serpentine ores results in more CO_2 generated than sequestered, or zero CO_2 avoided. Both cases argue for alternative means to improve mineral reactivity, such as improved reactor design.

Progress in Reactor Design

The ARC aqueous mineral-carbonation process has been demonstrated using a batch autoclave with continuous stirring and constant temperature and P_{CO2} capability. An industrial-scale process clearly requires continuous processing, and the elevated P and T conditions make reactor design a critical issue. Because required wall thickness for a pressure vessel is directly related to pressure and diameter, large-scale conventional autoclave reactors operating at 150 atm would be extremely thick-walled and very capital intensive. An ideal reactor design would entail minimal diameter to limit wall thickness without limiting scale. A continuous pipeline reactor meets these criteria for the current aqueous mineral carbonation process; a conceptualized view of such a reactor is shown in Figure 5.

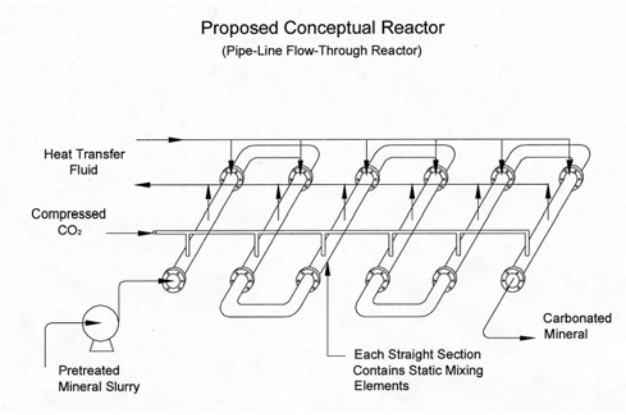

Figure 5. Conceptual pipeline reactor.

A research prototype loop reactor was conceived that would permit operation in the pipeline design without the need to build a full-scale reactor. Figure 6 shows the loop reactor constructed at ARC prior to installation of insulation. The design, construction, and operation are discussed in more detail by Penner et al. (2003 a,b).

The first prototype high-temperature, high-pressure (HTHP) flow-loop reactor serves as a technical bridge between batch autoclave tests and construction and operation of true continuous research reactor. Tests with a flow loop model can aid in proving the concept of reaction via pipeline and help acquire the engineering data needed for the design and construction of a continuous pipeline reactor.

However, before any discussion of construction of a second-generation pipeline reactor was warranted, a feasibility study of the current aqueous mineral carbonation process was necessary.

A mineral carbonation feasibility study was commissioned by the National Energy Technology Laboratory (NETL) and completed by Lyons et al. (2003), using a preliminary process design and basis developed at ARC by Nilsen and Penner (2001). A steady-state simulation of the process was created in Aspen® process simulation software, from which capital- and operating-cost estimates were generated. This study evaluated an olivine-based mineral-carbonation process scaled for the sequestration of 100% of the CO_2 emissions from a 1.3 GW coal-fired power plant. Olivine was selected as the mineral reactant in part to simplify the process by eliminating the heat-pretreatment stage.

Figure 6. HTHP Flow-Loop Reactor.

Because the proposed pipeline reactor design referred to above was unproven at the time, a conservative approach was adopted and conventional continuous-flow leach-type autoclave reactors were selected for the study. The impact of the conventional reactor design on the process economics is significant. The design required 95 reactor vessels, of 14-foot diameter, 87-foot length, with 14-inch thick walls, which accounted for roughly 50% of total capital costs.

The NETL study evaluated sequestration of approximately 1,100 tons of CO_2 per hour, requiring roughly 2,500 tons of virgin olivine ore plus an additional 800 tons of olivine from an unreacted product recycle loop every hour. Power requirements total 352 MW, with nearly 75% of the total power required for the ore-grinding operations. This power represents a 27% energy penalty on the power plant for which the sequestration operation was designed. Sensitivity analyses were conducted to evaluate the impact of reduced reactor residence time and P_{CO2} on the overall sequestration cost and energy demand. These results were used to derive the carbonation costs for the alternative mineral feedstocks described by O'Connor et al. (2004), as well as the overall carbonation costs and CO_2 balance by mineral-carbonation region.

The report from this study concluded that the cost of sequestration for this process is $69 per ton of CO_2. This economic cost cannot justify its primary benefit, superior stability to other proposed methods of CO_2 sequestration, unless it can be reduced by improvements to the process. Improved reactor design is the most promising route to cutting both the capital and operating costs for this mineral carbonation process.

Proof of concept of flow reactor

The initial round of tests with the HTHP flow-loop reactor showed that adequate mixing and contact between the various reactants can be achieved with olivine resulting in good reactivity. Several aspects of this reactor differ substantially from autoclave reactors. Mixing of slurry and supercritical CO_2 in an autoclave is accomplished by providing a constant pressurized blanket of CO_2 over the top of a stirred slurry. The impeller has a hollow core that allows the CO_2 blanket to be drawn down through the shaft and dispersed into the slurry to provide a constant supply of CO_2 to make up for depleted reactant. A flow-loop reactor provides this multiphase contact primarily by the mixing provided by flow and structure in the pipe that disturbs or redistributes the phases. A higher degree of mixing is accomplished by higher flow rates and by inserting static mixers in the pipe. Because the slurry is 6 to 7 times denser than the CO_2 at operating conditions there is a tendency for the dispersed CO_2 bubbles to coalesce into larger bubbles if flow rates are too low or mixing structure is unavailable. Coalesced CO_2 results in a change from

turbulent well-mixed flow to other operating regimes such as slug- or stratified flow where reaction rates may be impeded. See figure 7 for a diagram of changing flow regime. The challenge is to balance the

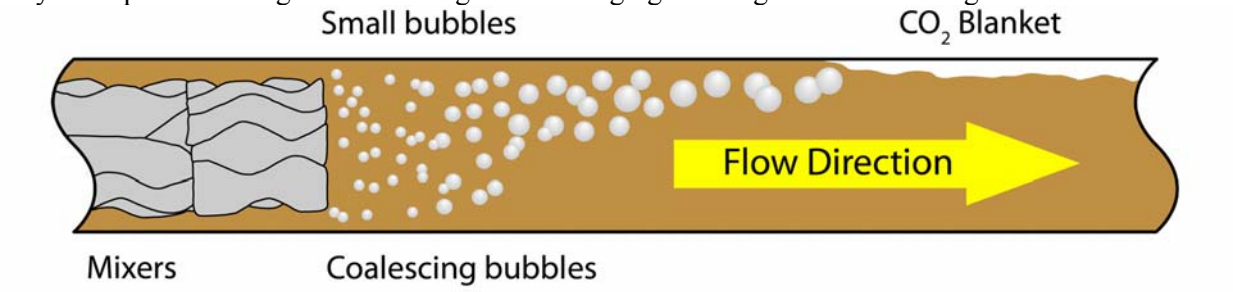

Figure 7. Conceptualization of CO2 and slurry flow through a pipe.

amount of flow and mixing necessary to prevent solids from silting out and create a vigorous reaction in the pipe while minimizing the pumping energy and wear-inflicted damage to the system. First, it was necessary to determine the ratio of CO_2-to-slurry to promote efficient reactivity.

Effect of CO_2/slurry volume ratio

For these tests a 15% (by weight) olivine slurry feed was chosen. In addition, a full set of six static mixers was placed in the pipe. Initial tests with the reactor began with a nearly full reactor, approximately 2L of slurry. Carbonation was very low, less than 10% extent of reaction. We concluded that the high level of slurry in the reactor forced the lighter gas/supercritical fluid phase of CO_2 into the upper portions of the reactor that were not in the direct flow through the pipes. Without continuous, intimate contact with the slurry, very little conversion could result. In subsequent tests, the reactor was under-filled to varying degrees to create a gas cavity that would force CO_2 to be circulated through the pipes with the mineral slurry. Less than 1.5 L of slurry caused voids that compromised the ability of the pump to move the slurry. A series of tests was conducted using several fill volumes (standard test conditions: 185°C, 150 atm P_{CO2}, 1 hr reaction, $NaHCO_3$/ NaCl aqueous carrier.) The carbonation results are shown in figure 8 as a function of fill volume. The olivine used in the these tests was wet-attrited at a 5:1 media:charge ratio to activate the mineral (D_{50} = 3.9μm). (Extent of reaction calculations shown in figure 8 are based on carbonation of Mg only, and thus are not directly comparable to those shown in table 1 where extent-of-reaction numbers are lowered slightly by the inclusion of Ca and Fe.) Based on estimated volumes of gas and slurry, the gas-to-slurry ratio for best reaction rates is about 5 to 15%, corresponding to the values for 1.7, 1.8, and 1.9 L reactor fill.

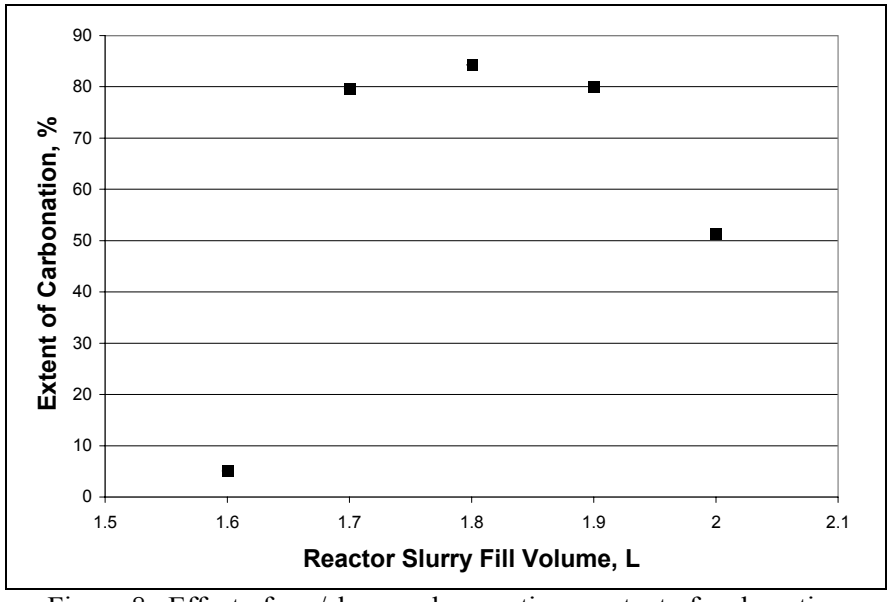

Figure 8. Effect of gas/slurry volume ratio on extent of carbonation reaction.

Enhanced reactivity compared with the autoclave

The tests described in figure 8 used an activated feed similar to that shown in tables 3 and 4 as the code 1C material. Table 3 shows that the parasitic energy loss for this level of activation is high - 55%. Two coarser feed materials were tested in the HTHP reactor. These correspond to the 1A and 1B material in milling and particle size, but they differed in storage to the extent that they had become passivated to reaction in the autoclave. The minus 400-mesh (D_{50} = 14μm) olivine feed reacted to

only 4.2% of its theoretical extent in one hour at the normal HTHP conditions. When processed in the flow reactor, however, this material attained a much higher extent of reaction.

To push the capabilities of the flow loop reactor further, an even coarser ore was tested (minus 200 mesh). Several tests were conducted, the only variable being flow rate as measured by pump speed. In each test, the reactor was warmed up as usual with the slurry circulating at 1198 rpm pump speed. True flow rates are unknown, but the best estimate is about 2.6 gpm (3.6 fps). Just prior to adding high pressure CO_2 when the reactor reached 185°C, the pump speed was adjusted to a predetermined value and held at that value for the remainder of the run. Those four pump speeds in rpm were 1002, 1198, 1450, and 1750. See table 6 for extent of carbonation values for these tests and figure 9 for a graphic comparison of the reactivity as a function of pump speed for the 6-mixer reactor and 15% solids density. The reaction rates exceeded 63% at each of the flow rates even with the much coarser ore. This lends support to the idea that extensive, energy-intensive grinding of olivine is unnecessary for a reactor that maintains sufficient turbulence.

Table 6. Effect of pump speed on extent of carbonation.

Pump Speed, rpm	Static Mixers	Solids density, %	Grind size	Extent of Reaction, %
1198	6	15	< 400 mesh	72.0
1750	6	15	< 200 mesh	77.9
1198	6	15	< 200 mesh	63.2
1450	6	15	< 200 mesh	73.8
1002	6	15	< 200 mesh	66.9
1198	0	15	< 200 mesh	37.5
1002	0	15	< 200 mesh	47.1
1198	0	30	< 200 mesh	48.9
1450	0	30	< 200 mesh	51.2
1750	0	30	< 200 mesh	45.7

Even though the range of pump speeds increased from 1002 rpm to 1750 rpm, (2.2 to 3.8 gpm) the increase in reactivity was only minor and not perfectly correlated. Although more tests are needed to estimate the energy requirements for pumping slurry, pumping energy may be lower than the grinding energy requirements to reduce particle size from minus 200 mesh to minus 400 mesh or smaller for reaction in an autoclave. In addition, the autoclave method has its own slurry pumping costs.

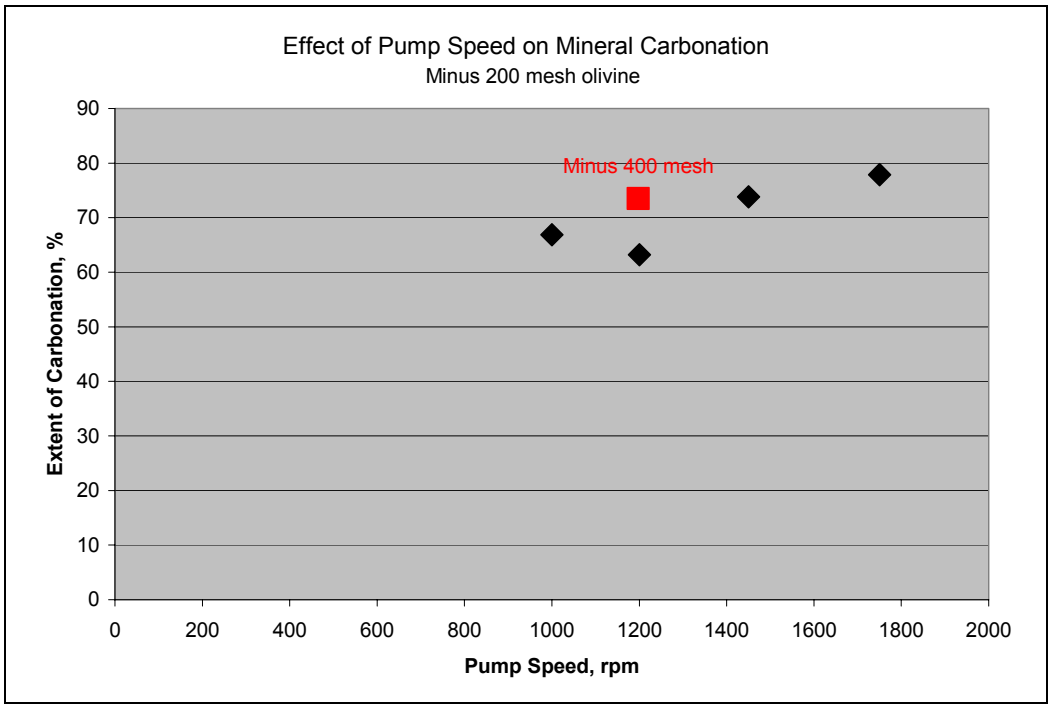

Figure 9. Effect of pump speed on extent of carbonation.

Compared to a stirred autoclave reactor, the enhanced reactivity of coarse ores in the flow-loop reactor was unexpected. More work is needed to understand this effect, but we have a hypothesis as to its cause. Turbulence may be greater in the loop reactor than in a stirred autoclave. This causes more collisions between particles and structure in the pipe. Other work has shown that the reaction starts with Mg ions being dissolved into the carrier and then precipitated as carbonates on the particle surface. Both

the product and the silica deposits left behind may hinder further Mg dissolution. In the turbulent environment of the flow loop reactor, the high-energy particle-to-particle interactions may rub off surface reaction products and expose fresh surfaces to further Mg dissolution and reaction.

If this is so, it is unknown whether the effect is limited to the zone of highest turbulence, in the pump, or whether it occurs in the nearly-as-turbulent mixer zones and in the straight sections of the pipe. To learn more about this effect, two tests were run under the same conditions, but with no static mixers. Results for these two tests, also in table 6, show lower reactivity in the mixerless pipe, 37.5% and 47.1% extent of reaction. Three tests were conducted in the mixerless pipe with higher solids content – 30%. Each of these tests was aborted less than halfway through the one-hour reaction time due to stalled flow in the pipe. Despite early termination, each test resulted in greater than 45% extent of reaction (table 6).

Reaction induced changes in slurry volume

Based on the results shown in figure 8, all of the tests summarized in table 6 were conducted using an estimated initial gas/slurry ratio of 1:9 by volume. It should be noted that a successful carbonation reaction produces additional solid product that occupies more volume in the reactor. This results in a lower gas/slurry ratio as head space in the pipe diminishes. Calculations were made for a 15% solids feed with 70% extent of reaction to determine the final slurry volume increase. The reaction product solids were measured for specific gravity (3.1) as was the feed material (specific gravity 3.36). Based on these measurements and the known stoichiometric change in mass, the volume of product would expand about 2.7%. A similar calculation can be made with the 30% solids feed. At only 50% extent of reaction the volume of the product slurry expands about 3.4%.

The thermal expansion of water is even more significant than the increase in solids. If the saline solution expands with temperature at the same rate as water, this would represent an 11% increase from ambient conditions to operating conditions. Taken together these two effects in the existing flow-loop reactor configuration, this slurry expansion causes the level in the reactor to force the lighter CO_2 phase into the upper portions of the reactor that are not in the direct flow through the pipes. These calculations demonstrate that initial fill conditions and solids densities are not static in this reactor and that a reaction can be self-extinguishing if the slurry volume expands too much. This analysis does not hold for a continuous reactor because the pipe has no out-of-flow headspace for the CO_2. The energy and volume contribution of CO_2 injection in a continuous flow pipe would instead contribute to its overall flow rate.

Effect of mixer design on reactivity

The results in table 6 show that removing mixers from the system dropped the reactivity from the 63-78% range to the 37-47% range. The mixers are effective for promoting good mixing and reactivity, but they have two important problems associated with their use. They contribute a significant pressure drop across the pipe and thus require substantial extra pumping energy in a continuous system. In addition, their twisting, weaving design promoted clogging in several of the tests. The flow-loop reactor simulates the action of a continuous reactor, but it remains a batch reactor device. As a result, any given region in the pipe is exposed to a variety of test conditions during the run; e.g.; heat-up, cool-down, early reaction, late reaction, draining, washing, full, and empty. This is not generally true for a continuous reactor where the reaction section is always the reaction section, the cool-down section is always the cool-down section, and the pipe remains full of the CO_2/slurry during extended operation. Scale build-up and clogging were observed during operation of the reactor especially in the mixer sections. This was first evident during runs when the differential pressure meters detected increased pressure drop across mixer segments. To prevent the build-up of solids from hampering the reactor flow rates significantly, it was necessary to remove and clean them frequently. The solids are not easily dislodged, but ultrasonic cleaning was effective, and normal pressure drop signals were detected after the mixers were reinstalled and operated in subsequent runs.

It should not be assumed, however, that the buildup of solids in the mixers would be expected in a continuous system. The multiple environments in the flow-loop reactor, described earlier, may promote much more scale or chunk formation than a continuous reactor with its steady-state regime. This can only be determined by operating a continuous reactor. To increase reactivity from mixerless design and prevent the clogging experienced with the current mixers, we intend to test a different mixer design. See the ribbon-type mixer in figure 10 shown next to the current mixer design.

Figure 10. Static mixer used for this study (top), to be tested (bottom).

Challenges in reactor design

A key parameter for the HTHP flow-loop reactor is slurry flow velocity. Two separate non-invasive flow meters that clamp to the outside of the pipe are yielding inconsistent data, and many times deliver no signal at all. The manufacturer warned that the stainless steel pipe used in the system is prone to ringing the signal around the pipe. In addition, audio and electronic noise can interfere with effective operation.

A significant effort was made to re-evaluate the meters that are commercially available. Most of these meters are not rated for the high-temperature, high-pressure conditions found in the reactor. Several varieties that use pressure drop measurements rely on knowledge of the fluid's properties to calibrate the meter. But the apparent viscosity and density of the mixed fluids (mineral solids, salt solution, supercritical CO_2) are not known. A model first proposed by Lockhart and Martinelli (1949) illustrates how the addition of gases can increase a fluid's resistance to flow. Apparent viscosity increases with addition of gases or supercritical CO_2. When CO_2 is added to flowing slurry, at constant flow, a substantial additional frictional pressure drop results. At constant pumping energy, this means that a significant drop in slurry flow rate would be expected. See table 7 to see how this plays out in a circuit under the conditions used in the flow loop reactor.

Table 7. Modeled values for Lockhart-Martinelli calculation for mineral carbonation for various ratios of mineral slurry to CO_2, designed to yield constant pressure drop losses for 100 feet of schedule 80, ½" stainless steel pipe. Temperature 185°C, Pressure 2375 psig. Estimated slurry viscosity 0.8 cP.

Slurry Flow Rate, gpm	Gas Flow Rate, lbs/hr	Delta P for 100 ft, psig	Reynolds #	Liquid Volume Holdup Fraction
2.8	0.01	10.16	26,900	.985
2.55	5	10.23	24,500	.869
2.0	21	10.16	19,300	.709

Notice from table 7 that if frictional pressure drop is held constant, even small quantities of CO_2 cause a significant loss of slurry flow. Note also that in the HTHP reactor, without an accurate measurement of volume occupied by the CO_2 phase in the pipe, no useful measurement of slurry flow can be made that depends on constant transport properties. The two sources of expansion discussed above are also complicating factors. When the HTHP flow-loop reactor begins its pre-heating stage, the liquid volume holdup fraction increases, and the apparent gas flow rate decreases in the reactor. This causes a change in apparent viscosity of the mixed phases. The effect is further influenced by the onset of reaction and the subsequent expansion of the slurry from mixed solids. Another factor that affects apparent viscosity is the increase in slurry density that results from the mineralization of CO_2. In the two examples listed above, the 15% solids feed would experience an 8.3% increase in viscosity, and the 30% solids feed would increase viscosity by 15.1%.

Modeling the process is further complicated by the inability to accurately measure volume inside the reactor. The system has several dead areas where solids can silt out and accumulate. Scaling on pipe structure also reduces the volume. Measured volumes are therefore imprecise and change from test to test, and this can affect the estimation of gas flow rate and liquid volume holdup fraction.

Despite the absence of accurate metering, progress has been made in estimating system flow. The manufacturer of the mixers provided estimated pressure drop data for water for a 4 gpm flow rate. This only works while the mixer is free from solids accumulation. Realizing that pressure, temperature, slurry densities, and added gas effects all have an effect on viscosity, the value for water was assumed as a proxy for the multiphase fluids. From this we have obtained an estimated flow of 2.6 gpm at 1198 rpm. This is not far from a frequent reading obtained from the existing flow meters when they are able to record a consistent signal.

Reactor component wear

The HTHP flow-loop reactor was operated for 27 tests that averaged at least 4 hours at HTHP conditions pumping mineral slurries. Operation exceeded 100 hours at these extreme conditions and at least another 100 hours pumping low- and no-solids solutions for cleaning and calibration tests. The last three runs resulted in stalled flows and were particularly stressful to the pump, and the last test ended in a clatter of pump bearings and shaft failure. The damaged shaft is shown in figure 11.

Evidence of wear from the slurry was found on the pump impeller (figure 12) and the cut water between the two pump ports (figure 13). Significant wear was expected on these parts, but it is not known whether it was accelerated by the multiple flow regimes and environments unique to the flow-loop reactor. Changes were noted in the static mixers after similar periods of operation. Close inspection of the

Figure 11. Photo of broken pump shaft.

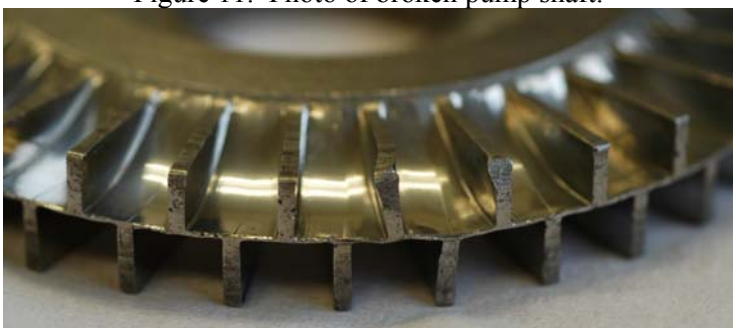

Figure 12. Worn pump impeller.

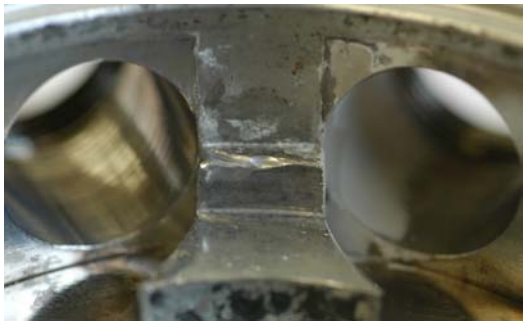

Figure 13. Wear on cut water near ports.

mixers showed very little observable wear (figure 14). Most of the observable changes came from scaling of solid reactor products on the mixer surfaces.

Figure 14. Static mixers before (left) and after (right) use in reactor.

One part of the reactor was subject to more wear than any other. The drain valve for the reactor is opened for a short time at the end of the run. When the cooling stage reaches a temperature of 85°C and the pressure has dropped to about 1500 psig, the valve is opened and the contents drained. The high pressure causes high-velocity slurry to pass quickly through a small aperture. Figure 15 shows the worn ball seat and valve that result from this operation. A continuous reactor would be designed with a properly sized orifice in the pressure-relief tank to minimize this effect.

Reactor plugging and stalled flow

The most significant problem in this round of testing was plugging and stalled flow in the pipe. The mechanism for these problems is not known. Post-test observation of various reactor parts shows that

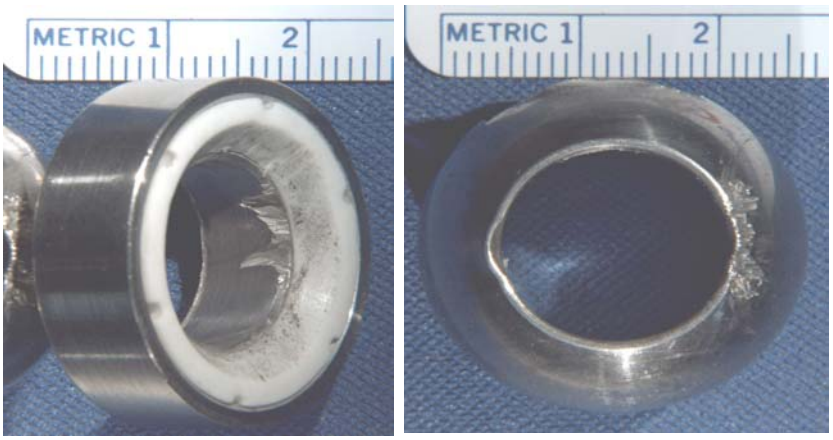

Figure 15. Worn ball valve parts.

several parts of the system are prone to scaling. It is not clear when in the reactor operation sequence the scale forms on components, but the multiple flow regimes that the pipes encounter are not necessarily the same as those that would define the operation of a continuous reactor. Mixers were frequently found after tests with substantial blockage from pieces of scale that had formed elsewhere in the reactor, broken off during test runs, and were caught in the reduced confines of the mixers. This was observable during operation, because the mixer pressure-drop reading fluctuated in response to plugging. Sometimes the pressure-drop data made significant changes quickly, when scale pieces would reorient or break free. This type of build-up in mixers undoubtedly caused changes in flow throughout the reactor.

Figure 16. Stalled flow solids (top) and pipe scale (bottom).

Flow stalling was observed in all three of the high slurry-density tests. The fragments of a solid plug from one of these tests are shown in figure 16. They are chemically similar to normal post-run products. At the bottom of figure 16 are two darker fragments of scale from the reactor. These typically had a lower carbonated content than the reactor products. The mechanism of flow stalling is also unknown. It is possible that the stall resulted from reduced flows resulting from previously aborted runs that left partial solid blockages in various parts of the system. The pump is being rebuilt with new parts in anticipation of further tests.

Conclusions

Carbon sequestration by mineral carbonation is inherently more expensive than some other sequestration technologies because it includes mining and ex situ processing costs. The high capital costs of processing by continuous autoclave reactors led to two research approaches for cutting costs. The first approach is to activate the mineral by pretreatment of olivine by grinding and by heat-activation for serpentines. The energy and cost penalties of these pretreatment methods are quantified in this study. Resulting parasitic energy losses for heat-treating serpentine were found to be near or in excess of the total plant energy. Parasitic energy losses for ultrafine grinding are in excess of 50% of the total plant energy. These energy requirements result in significant reductions in the net CO_2 avoided, from roughly 76% under standard pretreatment methodologies, to 40% with mechanical activation of the olivine and wollastonite ores, and 0% with heat activation of the serpentine ores.

The second approach to cutting capital costs is to improve the reactor design. An HTHP flow-loop reactor was designed and tested for mineral carbonation of olivine. Tests with coarse ore showed that reactivity in the flow-loop reactor was enhanced compared to reactivity results from stirred autoclave tests. The method is promising for cutting costs of mineral carbonation, but several design challenges must be overcome. These include accurate flow measurement, slurry flow stalling, reactor clogging, mixer design, and excessive wear of components subject to contact with slurry.

References

Barnes, V.E., Shock, D.A., and Cunningham, W.A. (1950). Utilization of Texas Serpentine. The University of Texas, Bureau of Economic Geology, No. 5020.

Bond, F.C. (1952). The Third Theory of Comminution. *Transactions*, *AIME*, vol. 193, p. 484, American Institute of Mining, Metallurgical, and Petroleum Engineers, Inc., New York.

Bond, F.C. (1985). "Testing and Calculations," in Sec. 3A: "General Aspects of Comminution," SME Mineral Processing Handbook, Weiss, N.L., ed., Society of Mining Engineers of the American Institute of Mining, Metallurgical, and Petroleum Engineers, Inc., New York, pp. 3A-16-3A-27.

Chizmeshya, A.V.G., McKelvy, M.J., Sankey, O.F., Wolf, G.H., Sharma, R., Bearat, H, Diefenbacher, J., and Carpenter, R.W. (2002). Atomic-Level Understanding of CO_2 Mineral Carbonation Mechanisms from Advanced computational Modeling. Proc., 27th International Technical Conference on Coal Utilization and Fuel Systems, Coal Technology Association, Clearwater, FL.

Goff, F., Guthrie, G., Lipim, B., Chipera, S., Counce, D., Kluk, E., and Ziock, H. (2000). Evaluation of the Ultramafic Deposits in the Eastern United States and Puerto Rico as sources of Magnesium for Carbon Dioxide Sequestration, Los Alamos National Laboratory, LA-13694-MS, 36 pp.

Govier, D. and Arnold, M. (2004). Quantitative Differential Thermal Analysis of Antigorite and Lizardite Serpentine, Internal Report, Albany Research Center Analytical Laboratory.

King, E.G., Barany, R., Weller, W.W., and Pankratz, L.B. (1967). Thermodynamic Properties of Forsterite and Serpentine, U.S. Bureau of Mines, RI 6962.

Lockhart and Martinelli. (1949). Chem. Eng. Prog., 45, 39-48 also found in Perry's Chemical Engineers Handbook, Sixth Ed., page 5-41.

Lyons, J.L., Berkshire, L.H., and White, C.W. (2003). Mineral Carbonation Feasibility Study, Draft Report, Commissioned by National Energy Technology Laboratory, 56 pp.

McKelvy, M.J., Chizmeshya, A.V.G., Bearat, H., Sharma, R., and Carpenter, R.W. (2001). "Developing Mechanistic Understanding of CO_2 Mineral Sequestration Reaction Processes," Proc. 26th International Tech. Conference on Coal Utilization & Fuel Systems, Clearwater, FL, March 5-8, pp. 777-788.

McKelvy, M.J., Chizmeshya, A.V.G., Bearat, H., Diefenbacher, J., Sharma, R., Carpenter, R.W., and Wolf, G. (2002). Developing a Mechanistic Understanding of Serpentine CO_2 Mineral Carbonation Reaction Processes. Proc., 27th International Technical Conference on Coal Utilization and Fuel Systems, Coal Technology Association, Clearwater, FL.

Nilsen, D.N. and Penner, L.R. (2001). Reducing Greenhouse Gas Emissions: Engineering and Cost Assessment of Direct Mineral Carbonation Technology (Process Development Information for the Olivine Process). Albany Research Center, Office of Fossil Energy, US DOE, DOE/ARC-TR-01-015.

O'Connor, W. K., Dahlin, D.C., Rush, G.E., Dahlin, C.L., and Collins, W.K. (2001). "Carbon Dioxide Sequestration by Direct Mineral Carbonation: Process Mineralogy of Feed and Products," Preprint No. 01-9, SME Annual Meeting, Denver, CO, Feb. 26-28, 9 p.

O'Connor, W.K., Dahlin, D.C., Nilsen, D.N., Gerdemann, S.J., Rush, G.E., Walters, R.P., and Turner, P.C. (2001). "Research Status on the Sequestration of Carbon Dioxide by Direct Aqueous Mineral Carbonation," Paper 35-1, Proc. 18th Annual Inter. Pittsburgh Coal Conference, Newcastle, NSW, Australia, December 3-7, 11 pp.

O'Connor, W.K., Dahlin, D.C., Nilsen, D.N., Gerdemann, S.J., Rush, G.E., Penner, L.R., Walters, R.P., and Turner, P.C. (2002). "Continuing Studies on Direct Aqueous Mineral Carbonation for CO2 Sequestration," Proc. 27th International Tech. Conference on Coal Utilization & Fuel Systems, Clearwater, FL, March 4-7.

O'Connor, W.K., Dahlin, D.C., Rush, G.E., Gerdemann, S.J, Penner, L.R., and Nilsen, D.N. (2004). "Aqueous Mineral Carbonation: Mineral Availability, Pretreatment, Reaction Parametrics, and Process Studies," US DOE, DOE/ARC-TR-04-002.

Penner, L.R., Gerdemann, S.J., Dahlin, D.C., O'Connor, W.K., Nilsen, D.N. (2003). "Progress on Continuous Processing for Mineral Carbonation Using a Prototype Flow Loop Reactor," Proc. of the 28th Inter. Tech. Conf. on Coal Util. & Fuel Systems, Clearwater, FL, March 9-13, 12 pp.

Penner, L.R., O'Connor, W.K., Gerdemann, S.J., and Dahlin, D.C. (2003). "Mineralization Strategies for Carbon Dioxide Sequestration," 20th Annual International Pittsburgh Coal Conference, Pittsburgh, PA, September 15-19, 19 pp.

U.S. Bureau of Mines, Staff. (1987). Bureau of Mines Cost Estimating System Handbook (in Two Parts). Part 1. Surface and Underground Mining, IC 9142, 631 pp. Part 2. Mineral Processing, IC 9143, 565 pp.

Virta, R.L. (2001). Wollastonite, U.S. Geological Survey Minerals Yearbook –2001.

Zhang, Q., Sugiyama, K., and Saito, F. (1996). "Enhancement of Acid Extraction of Magnesium and Silicon from Serpentine by Mechanochemical Treatment." Hydrometallurgy, vol. 45, pp. 323-331.